Video Article

Label-Free Identification of Lymphocyte Subtypes Using Three-Dimensional Quantitative Phase Imaging and Machine Learning

Jonghee Yoon[1], YoungJu Jo[2,3,4,7], Young Seo Kim[3,4,5], Yeongjin Yu[2,3], Jiyeon Park[6], Sumin Lee[4], Wei Sun Park[2,3], YongKeun Park[2,3,4]

[1]Department of Physics, University of Cambridge

[2]Department of Physics, Korea Advanced Institute of Science and Technology

[3]KAIST Institute for Health Science and Technology, Korea Advanced Institute of Science and Technology

[4]Tomocube, Inc.

[5]Department of Chemical and Biomolecular Engineering, Korea Advanced Institute of Science and Technology

[6]Department of Biological Sciences, Korea Advanced Institute of Science and Technology

[7]Department of Applied Physics, Stanford University

Correspondence to: YongKeun Park at yk.park@kaist.ac.kr

URL: https://www.jove.com/video/58305
DOI: doi:10.3791/58305

Keywords: Immunology and Infection, Issue 141, Quantitative phase imaging, optical diffraction tomography, holotomography, holographic microscopy, lymphocyte identification, immune cell, immunology, machine learning, label-free imaging

Date Published: 11/19/2018

Citation: Yoon, J., Jo, Y., Kim, Y.S., Yu, Y., Park, J., Lee, S., Park, W.S., Park, Y. Label-Free Identification of Lymphocyte Subtypes Using Three-Dimensional Quantitative Phase Imaging and Machine Learning. *J. Vis. Exp.* (141), e58305, doi:10.3791/58305 (2018).

Abstract

We describe here a protocol for the label-free identification of lymphocyte subtypes using quantitative phase imaging and machine learning. Identification of lymphocyte subtypes is important for the study of immunology as well as diagnosis and treatment of various diseases. Currently, standard methods for classifying lymphocyte types rely on labeling specific membrane proteins via antigen-antibody reactions. However, these labeling techniques carry the potential risks of altering cellular functions. The protocol described here overcomes these challenges by exploiting intrinsic optical contrasts measured by 3D quantitative phase imaging and a machine learning algorithm. Measurement of 3D refractive index (RI) tomograms of lymphocytes provides quantitative information about 3D morphology and phenotypes of individual cells. The biophysical parameters extracted from the measured 3D RI tomograms are then quantitatively analyzed with a machine learning algorithm, enabling label-free identification of lymphocyte types at a single-cell level. We measure the 3D RI tomograms of B, CD4+ T, and CD8+ T lymphocytes and identified their cell types with over 80% accuracy. In this protocol, we describe the detailed steps for lymphocyte isolation, 3D quantitative phase imaging, and machine learning for identifying lymphocyte types.

Video Link

The video component of this article can be found at https://www.jove.com/video/58305/

Introduction

Lymphocytes can be classified into various subtypes including B, helper (CD4+) T, cytotoxic (CD8+) T, and regulatory T cells. Each lymphocyte type has a different role in the adaptive immune system; for example, B lymphocytes produce antibodies, whereas T lymphocytes detect specific antigens, eliminate abnormal cells, and regulate B lymphocytes. Lymphocyte function and regulation is tightly controlled by and related to various diseases including cancers[1], autoimmune diseases[2], and viral infections[3]. Thus, the identification of lymphocyte types is important to understand their pathophysiological roles in such diseases and for immunotherapy in clinics.

Currently, methods for classifying lymphocyte types rely on antigen-antibody reactions by targeting specific surface membrane proteins or surface markers[4]. Targeting surface markers is a precise and accurate method to determine lymphocyte types. However, it requires expensive reagents and time-consuming procedures. Furthermore, it carries risks of the modification of membrane protein structures and the alteration of cellular functions.

To overcome these challenges, the protocol described here introduces the label-free identification of lymphocyte types using 3D quantitative phase imaging (QPI) and machine learning[5]. This method enables the classification of lymphocyte types at a single-cell level based on morphological information extracted from label-free 3D imaging of individual lymphocytes. Unlike conventional fluorescence microscopy techniques, QPI utilizes refractive index (RI) distributions (intrinsic optical properties of live cells and tissues) as optical contrast[6,7]. The RI tomograms of individual lymphocytes represent phenotypic information specific to subtypes of lymphocytes. In this case, to systemically utilize 3D RI tomograms of individual lymphocytes, a supervised machine learning algorithm was utilized.

Using various QPI techniques, the 3D RI tomograms of cells have been actively used for the study of cell pathophysiology because they provide a label-free, quantitative imaging capability[8,9,10,11,12,13]. Also, the 3D RI distributions of individual cells can provide morphological, biochemical, and biomechanical information about cells. 3D RI tomograms have been previously utilized in the fields of hematology[14,15,16,17],

infectious diseases[18,19,20], immunology[21], cell biology[22,23], inflammation[24], cancer[25], neuroscience[26,27], developmental biology[28], toxicology[29], and microbiology[12,30,31,32].

Although 3D RI tomograms provide detailed morphological and biochemical information of cells, the classification of lymphocyte subtypes is difficult to achieve by simply imaging 3D RI tomograms[5]. To systematically and quantitatively exploit the measured 3D RI tomograms for the cell type classification, we utilized a machine learning algorithm. Recently, several works have been reported in which quantitative phase images of cells were analyzed with various machine learning algorithms[33], including the detection of microorganisms[34], classification of bacterial genus[35,36], rapid and label-free detection of anthrax spores[37], automated analysis of sperm cells[38], analysis of cancer cells[39,40], and detection of macrophage activation[41].

This protocol provides detailed steps to perform label-free identification of lymphocyte types at the individual cell level using 3D QPI and machine learning. This includes: 1) lymphocyte isolation from mouse blood, 2) lymphocyte sorting via flow cytometry, 3) 3D QPI, 4) quantitative feature extraction from 3D RI tomograms, and 5) supervised learning for identifying lymphocyte types.

Protocol

Animal care and experimental procedures were performed under the approval of the Institutional Animal Care and Use Committee of KAIST (KA2010-21, KA2014-01, and KA2015-03). All the experiments in this study were carried out in accordance with the approved guidelines.

1. Lymphocyte Isolation from Mouse Blood

1. Once a C57BL/6J mouse is euthanized via CO_2 inhalation, insert a 26-G needle into the mouse heart and collect 0.3 mL of blood. Directly put blood into a tube with 100 U/mL heparin solution diluted with 1 mL of phosphate-buffered saline (PBS).
   NOTE: Alternatively, lymphocytes from the spleen can be isolated.
2. Centrifuge the tube at 400 x g for 5 min at 4 °C.
3. Add 0.5 mL of ammonium-chloride-potassium lysing buffer to the tube and gently invert it a few times to mix the solution.
4. Incubate the tube at room temperature (RT) for 5 min.
5. Wash the cells by adding 4.5 mL of PBS and centrifuging at 400 x g for 5 min at 4 °C, twice.
6. Remove the supernatant and resuspend the cell pellet in 100 µL of fresh RPMI-1640 medium with 10% fetal bovine serum (FBS).
7. Add 0.1 µg of CD16/32 (2.4G2) antibody to the tube for blocking.
8. Keep the tube on ice.

2. Flow Cytometry and Sorting of Lymphocyte Subtypes

NOTE: Sorting lymphocytes depending on cell type is essential for establishing the ground-truth (*i.e.,* correct) cell type labels to train and test a cell type classifier in supervised learning. Flow cytometry, a gold standard method, is used to identify and separate lymphocytes[42].

1. Make a mixture of surface marker staining antibodies in 100 µL of fresh RPMI-1640 medium [with 10% FBS, 0.1 µg of CD3e (17A2), CD8a (53-6.7), CD19 (1D3), CD45R (B220, RA3-6B2), and NK1.1 (PK136)] and 0.25 µg of CD4 (GK1.5) antibodies to target B, CD4+ T, and CD8+ T lymphocytes.
2. Add 100 µL of the antibody mixture to the cell suspension (obtained in step 1.8).
3. Incubate for 25 min on ice.
4. Wash the cells by adding 5 mL of PBS and centrifuging at 400 x g for 5 min at 4 °C, twice.
5. Resuspend the cell pellet in 5 mL of fresh RPMI-1640 medium with 10% FBS and 2.5 µg of DAPI (4',6-diamidino-2-phenylindole).
6. Collect each lymphocyte type separately with flow cytometry using the fluorescence levels of the markers described above. Simultaneously exclude dead cells using the DAPI signals.
   NOTE: Detailed protocols regarding flow cytometry-based cell sorting have been described previously[42].

3. 3D Quantitative Phase Imaging

1. Keep the sorted lymphocytes on ice throughout the imaging procedures, which should be completed within 5 h (since lymphocyte isolation from the mouse) to avoid cell damage and biochemical alterations.
2. Select a sorted cell type (among B, CD4+ T, and CD8+ T lymphocytes) and dilute the sample (obtained in step 2.6) to 180 cells/µL with RPMI medium for optimal imaging condition (*i.e.,* one cell per single field-of-view).
3. Load 120 µL of the diluted sample into an imaging chamber by slow injection. Thoroughly check on the presence of bubbles in the imaging chamber with the sample. If there are bubbles, carefully remove them, as they will compromise the quality of the measurements.
4. Acquire 3D RI tomograms using a commercial 3D quantitative phase microscope, or holotomography, and its imaging software.
   NOTE: Detailed information about the experimental setup can be found in the original manuscript[5].
   1. Place a drop of distilled water on top of the objective lens of the microscope.
   2. Place the imaging chamber with the sample on the translation stage of the microscope and adjust its location so that the sample aligns with the objective lens.
   3. Adjust the axial positions of the objective and condenser lenses by clicking **Focus** and **Surface**, respectively, on the "Calibration" tab of the "Microscope" perspective of the imaging software.
   4. Align the objective and condenser lenses by clicking **Auto Mode**. Alternatively, use **Scanning Mode** and manually adjust the lenses so that the illumination patterns are localized at the central region of the field-of-view.
   5. Return to **Normal Mode** and adjust the translation stage to locate a cell in the field-of-view.
   6. Find the focal plane by adjusting the axial position of the objective lens. Perfect focusing makes the sample boundary visualized in the screen almost invisible.

7. Adjust the translation stage to find a location without a cell.
8. Click **Calibrate** to measure multiple 2D holograms with varying illumination angles.
9. Adjust the translation stage to locate a cell at the center of the field-of-view.
10. Move to the "Acquisition" tab and click **3D Snapshot** to measure the holograms of the cell with the identical illumination angles as done in step 3.4.8.
11. When the acquired data is presented on the "Data Management" panel, right-click on the acquired data and click **Process** to reconstruct a 3D RI tomogram from the holograms measured in steps 3.4.8 and 3.4.10, using the diffraction tomography algorithm[9,10] implemented in the imaging software.
12. Repeat steps 3.4.5-3.4.11 to measure more than 100 cells to ensure statistical power for machine learning.
13. All images that are processed through the step 3.4.11. can be visualized. On the “Data Management” panel, right-click the data and click Open to visualize the data. Click RI Tomogram on the “Data Manager” panel. On the “Preset” tab, click Load and double click “lymphocyte.xml”, which is a predefined transfer function provided by the imaging software to visualize the tomogram according to the 3D RI distributions.

5. Repeat steps 3.2-3.4 to measure 3D RI tomograms of all lymphocyte subtypes.

4. Quantitative Morphological and Biochemical Feature Extraction from 3D RI Tomograms

1. Place all the tomographic data measured above in a single folder. Split the cell types in the subfolders of this folder. Prepare each tomogram to be a single *.mat* file.
2. Open **Supplementary File 1** - Feature Extraction (written for an image processing software).
3. Edit line 14 to designate the tomogram folder prepared in step 4.1.
4. Edit line 15 to designate a folder to save the extracted feature data.
5. Optionally, edit line 17 to adjust the RI threshold parameters for feature extraction. The default option is 20 RI thresholds from 1.340-1.378, with an increment of 0.002 as described previously[5].
6. Execute the code. For every tomogram in the dataset, the code calculates five features: surface area (SA), cellular volume (CV), sphericity (SI), protein density (PD), and dry mass (DM), per RI threshold. The detailed algorithms for feature extraction are described elsewhere[5].
7. In order to monitor the feature extraction, during the execution check on the screen visualizing RI threshold-based cell segmentation.
8. Check on the extracted feature data, as *.mat* file per tomogram, saved in the folder designated in step 4.4.

5. Supervised Learning and Identification

1. Randomly split the feature data obtained in step 4.8 to training (70%) and test (30%) sets with separate folders.
2. Open **Supplementary File 2** - Train (written for an image processing software).
3. Edit line 14 to designate the training set prepared in step 5.1.
4. Edit line 16 to designate a folder to save the trained classifier.
5. Edit line 17 to set a file name for the classifier.
6. Optionally, edit line 19 to select the features for training. The default option, as specified previously[5], was used to obtain the representative results below.
7. Execute the code. Using the selected features of the training set, the code trains a classifier with the *k*-nearest neighbor algorithm (*k*-NN; k = 4) and then saves the classifier (as named in step 5.5) in the folder designated in step 5.4.
8. Check on the screen visualizing the classifier performance and the cross-validation accuracy.
9. Optionally, train multiple classifiers with different feature combinations by repeating steps 5.5-5.7. Then choose the classifier with the highest cross-validation accuracy.
10. Open **Supplementary File 3** - Test (written for an image processing software).
11. Edit lines 14-15 to designate the trained classifier to be tested.
12. Edit line 17 to designate the test set prepared in step 5.1.
13. Execute the code. The classifier described above identifies the cell types of the individual lymphocytes in the test set.
14. Check on the screen visualizing the identification performance and the test accuracy.

Representative Results

Figure 1 shows the schematic process of the entire protocol. Using the procedure presented here, we isolated B (n = 149), CD4+ T (n = 95), and CD8+ T (n = 112) lymphocytes. To obtain phase and amplitude information at various angles of illumination, multiple 2D holograms of each lymphocyte were measured by changing the angle of illumination (from -60° to 60°). Typically, 50 holograms can be used to reconstruct a 3D RI tomogram, but the number of 2D holograms can be adjusted considering the imaging speed and quality. Amplitude and phase information of the measured holograms are retrieved using a field retrieval algorithm based on Fourier transform[43,44]. The 3D RI tomogram of each lymphocyte was reconstructed from multiple 2D retrieved phase and amplitude information at various angles of illumination using optical diffraction tomography algorithm. Details of image process and 3D RI tomogram reconstruction method can be found elsewhere[21,45].

Figure 2A-2C shows representative 3D rendered RI tomograms of B, CD4+ T, and CD8+ T lymphocytes by allocating different color schemes according to RI values via the imaging software. From the RI values, quantitative morphological (SA, CV, and SI) and biochemical (PD and DM) features were calculated (**Figure 2A-2C**). This result clearly demonstrates that 3D RI distribution enables quantitative analysis of morphological as well as biochemical information of lymphocytes.

Supervised machine learning was exploited to identify lymphocyte types at a single-cell level. The measured 3D RI tomograms were randomly split into 70% and 30% of training (B: 104, CD4+ T: 66, and CD8+ T: 77) and test (B: 45, CD4+ T: 29, and CD8+ T: 35) datasets, respectively. We optimized the classifiers to maximally utilize the cell-type-specific fingerprints encoded in the feature space. The total accuracy, sensitivity (true positive), and specificity (true negative) were calculated by comparing the classifier-predicted results and ground-truth cell types.

In order to demonstrate proof-of-concept of the proposed protocol, we performed supervised machine learning on three different cases: binary classification of (i) B and T lymphocytes and (ii) two T lymphocyte subtypes (CD4+ and CD8+), and (iii) multiclass classification of all lymphocyte types.

Figure 3 shows identification performance of optimized classifiers for training and test stages. The accuracy of the T and B lymphocyte classification was 93.15% and 89.81% for the training and test cases, respectively. The CD4+ and CD8+ T lymphocytes were statistically classified, and the accuracy was 87.41% and 84.38% for the training and test sets, respectively. Lastly, the accuracy of the multiclass cell type classifier was 80.65% and 75.93% for the training and test stages, respectively.

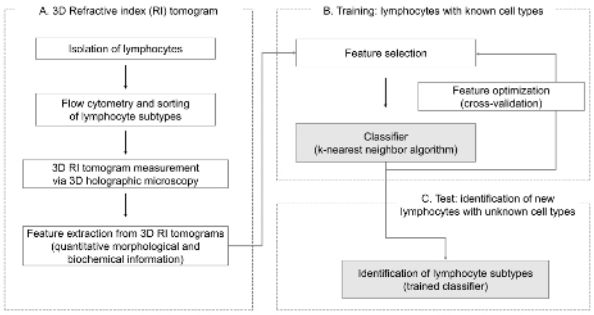

Figure 1: Schematic diagrams of the label-free identification of lymphocyte types exploiting 3D quantitative phase imaging and machine learning. Please click here to view a larger version of this figure.

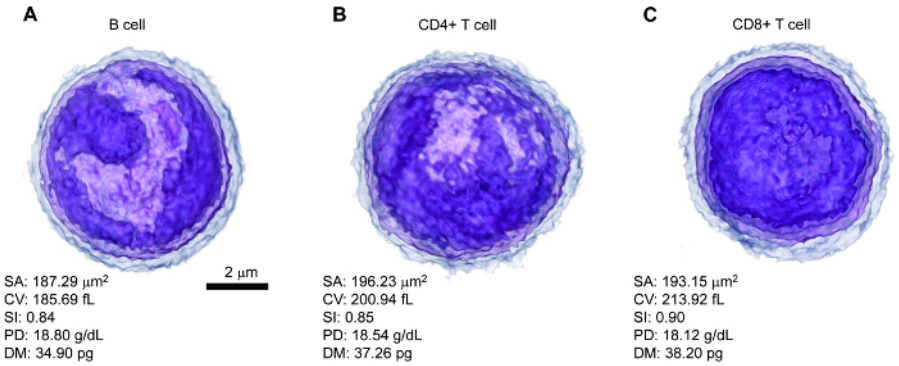

Figure 2: Representative 3D rendered RI tomograms of each lymphocyte cell type with quantitative morphological and biochemical features. (A) B cell, (B) CD4+ T cell, and (C) CD8+ T cell. Scale bar = 2 μm. SA, surface area; CV, cellular volume; SI, sphericity; PD, protein density; DM, dry mass. This figure is modified with permission[5]. Please click here to view a larger version of this figure.

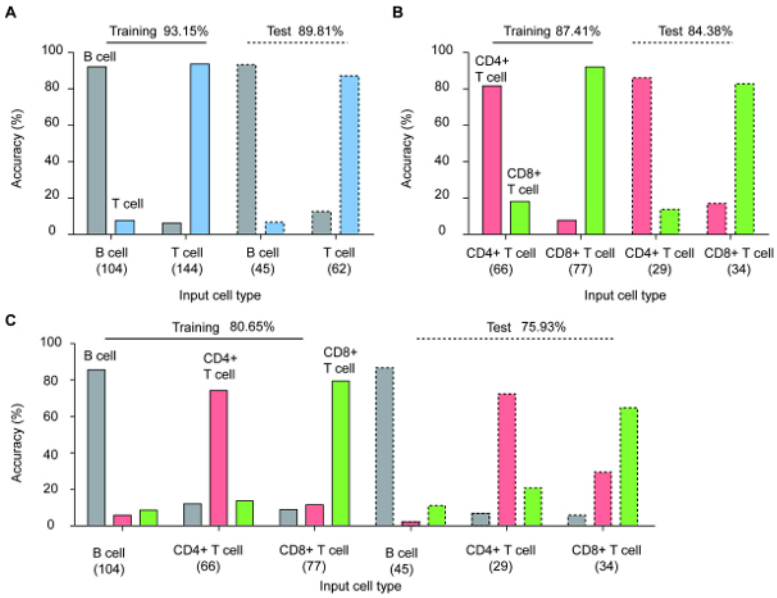

Figure 3: Identification of individual lymphocyte types via supervised machine learning (A) binary classification of B and T cells, (B) binary classification of CD4+ and CD8+ T cells, and (C) multiclass classification of all three lymphocyte cell types; for both training and test sets. Note the small difference between the training and test cases, suggesting nice generalization of the established classifiers. The numbers below the names of each cell type indicate the number of cells used. This figure is modified with permission[5]. Please click here to view a larger version of this figure.

Supplementary File 1: Feature extraction code. Extracting features (SA, CV, SI, PD, and DM) after RI threshold-based segmentation of each tomogram. Implemented in an image processing software. Please click here to download this file.

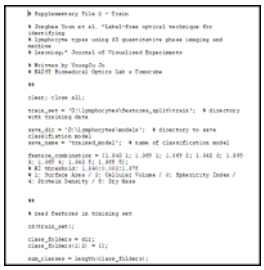

Supplementary File 2: Training code. Training a *k*-NN classifier training based on selected features. Implemented in an image processing software. Please click here to download this file.

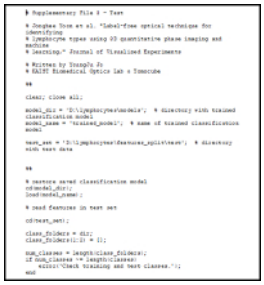

Supplementary File 3: Testing code. Testing a trained *k*-NN classifier for a new dataset (*i.e.*, test set). Implemented in an image processing software. Please click here to download this file.

Discussion

We present a protocol that enables the label-free identification of lymphocyte types exploiting 3D quantitative phase imaging and machine learning. Critical steps of this protocol are quantitative phase imaging and feature selection. For the optimal holographic imaging, the density of cells should be controlled as described above. Mechanical stability of the cells is also important to obtain a precise 3D RI distribution because floating or vibrational cellular motions will disturb hologram measurements upon illumination angle changes. We, therefore waited several minutes until the sample became stable and static in the imaging chamber before measuring holograms. Lastly, bubbles inside the imaging chamber are problematic when measuring holograms due to RI differences between air and the sample; thus, the sample should be carefully loaded to the imaging chamber.

Feature extraction and selection help determine the identification performance of the classifier. We calculated 5 quantitative morphological (CV, SA, SI) and biochemical (PD, DM) features from 3D RI distribution at 20 different RI threshold values; thus, we extracted a total of 100 features. We exhaustively searched optimal feature and classifier combinations, which show that the best cross-validation accuracy was selected. We tested 6 different machine learning algorithms, including *k*-NN (k = 4 and k = 6), linear discrimination analysis, quadratic discrimination analysis, naïve Bayes, and decision tree, and we found that *k*-NN (k = 4) showed the best identification performance. However, there is a chance to improve identification accuracy using other machine learning methods, including support vector machine and neuronal networks.

This protocol measures intrinsic optical properties via 3D quantitative phase imaging in order to identify lymphocyte types; thus, it does not require a labeling process based on antigen-antibody reactions used in fluorescence or magnetic bead-based cell-sorting techniques, which have risks of altering cellular function by modifying membrane protein structures. Moreover, the present method measures 3D RI distribution and provides 3D morphological and biochemical information about the cell, which cannot be obtained by a single-shot holography method[46]; therefore, the identification performance of the protocol is more accurate due to high-dimensional information.

A minor limitation of this protocol is the manual adjustment of the sample stage and required labeling process for supervised machine learning. We searched a lymphocyte by adjusting the manual translational stage and measured holograms, which are the most time-consuming steps. This limitation would be improved by employing an automated motorized stage or microfluidic channel devices. Regarding supervised learning, the known lymphocyte types are required to establish the optimal classifier; thus, we had to first isolate and identify lymphocyte cell types based on the antigen-antibody-based sorting technique. Nonetheless, this protocol still uses the intrinsic optical contrast of lymphocytes, and the labeling agents used to specify antibodies have negligible effects on the measured 3D RI signal. Therefore, the established classifier may be used for identifying lymphocytes in a label-free manner.

Although this protocol mainly utilizes phenotypes of lymphocytes by measuring 3D RI tomograms of individual cells, these 3D RI data can also be used in combination with other modalities addressing genotypes or proteomic information for better classification of subtypes. Recently, correlative microscopy techniques combining fluorescence imaging and QPI have been introduced[47,48,49]. The approach presented in this protocol can also be extended to these correlative imaging methods.

Label-free identification of lymphocyte types can be applied to studying pathophysiology or diagnosing disease by detecting abnormal lymphocytes or ratios among lymphocyte types. Furthermore, this protocol can be applied to whole blood analysis by identifying various cells including red blood cells, platelets, and white blood cells.

Disclosures

Prof. Y. Park, Y. Jo, Y. S. Kim, and S. Lee have financial interests in Tomocube, Inc., a company that commercializes optical diffraction tomography and quantitative phase imaging instruments and is one of the sponsors of the work.

Acknowledgements

This work was supported by the KAIST BK21+ Program, Tomocube, Inc., and the National Research Foundation of Korea (2015R1A3A2066550, 2017M3C1A3013923, 2018K000396). Y. Jo acknowledges support from the KAIST Presidential Fellowship and Asan Foundation Biomedical Science Scholarship.

References

1. Alizadeh, A. A., *et al.* Distinct types of diffuse large B-cell lymphoma identified by gene expression profiling. *Nature.* **403**(6769), 503 (2000).
2. Von Boehmer, H., Melchers, F. Checkpoints in lymphocyte development and autoimmune disease. *Nature Immunology.* **11**(1), 14 (2010).
3. Cirión, A., *et al.* HIV controllers exhibit potent CD8 T cell capacity to suppress HIV infection ex vivo and peculiar cytotoxic T lymphocyte activation phenotype. *Proceedings of the National Academy of Sciences.* **104**(16), 6776-6781 (2007).
4. Fischer, K., *et al.* Isolation and characterization of human antigen-specific TCRαβ+ CD4-CD8-double-negative regulatory T cells. *Blood.* **105**(7), 2828-2835 (2005).
5. Yoon, J., *et al.* Identification of non-activated lymphocytes using three-dimensional refractive index tomography and machine learning. *Scientific Reports.* **7**(1), 6654 (2017).
6. Popescu, G. *Quantitative phase imaging of cells and tissues.* McGraw Hill Professional, (2011).
7. Lee, K. *et al.* Quantitative phase imaging techniques for the study of cell pathophysiology: from principles to applications. *Sensors.* **13**(4), 4170-4191 (2013).
8. Kim, D., *et al.* Refractive index as an intrinsic imaging contrast for 3-D label-free live cell imaging. *bioRxiv.*106328 (2017).

9. Kim, K., *et al.* Optical diffraction tomography techniques for the study of cell pathophysiology. *Journal of Biomedical Photonics & Engineering.* **2**(2), (2016).
10. Wolf, E. Three-dimensional structure determination of semi-transparent objects from holographic data. *Optics Communications.* **1**(4), 153-156 (1969).
11. Kuś, A., Dudek, M., Kemper, B., Kujawińska, M., Vollmer, A. Tomographic phase microscopy of living three-dimensional cell cultures. *Journal of Biomedical Optics*. **19** (4), 046009 (2014).
12. Kim, T., *et al.* White-light diffraction tomography of unlabelled live cells. *Nature Photonics.* **8**(3), 256 (2014).
13. Simon, B., *et al.* Tomographic diffractive microscopy with isotropic resolution. *Optica.* **4**(4), 460-463 (2017).
14. Kim, Y., *et al.* Profiling individual human red blood cells using common-path diffraction optical tomography. *Scientific Reports.* **4**, (2014).
15. Park, H., *et al.* Measuring cell surface area and deformability of individual human red blood cells over blood storage using quantitative phase imaging. *Scientific Reports.* **6**, (2016).
16. Lee, S., *et al.* Refractive index tomograms and dynamic membrane fluctuations of red blood cells from patients with diabetes mellitus. *Scientific Reports.* **7 ,** (2017).
17. Merola, F., *et al.* Tomographic flow cytometry by digital holography. *Light-Science & Applications.* **6**, (2017).
18. Park, Y., *et al.* Refractive index maps and membrane dynamics of human red blood cells parasitized by Plasmodium falciparum. *Proceedings of the National Academy of Sciences.* **105**(37), 13730-13735 (2008).
19. Park, H., *et al.* Characterizations of individual mouse red blood cells parasitized by Babesia microti using 3-D holographic microscopy. *Scientific Reports.* **5 ,**10827 (2015).
20. Chandramohanadas, R., *et al.* Biophysics of malarial parasite exit from infected erythrocytes. *Public Library of Science ONE.* **6**(6), e20869 (2011).
21. Yoon, J., *et al.* Label-free characterization of white blood cells by measuring 3D refractive index maps. *Biomedical Optics Express.* **6**(10), 3865-3875 (2015).
22. Kim, K., *et al.* Three-dimensional label-free imaging and quantification of lipid droplets in live hepatocytes. *Scientific Reports.* **6 ,**36815 (2016).
23. Kim, D., *et al.* Label-free high-resolution 3-D imaging of gold nanoparticles inside live cells using optical diffraction tomography. *Methods.* (2017).
24. Lenz, P., *et al.* Multimodal Quantitative Phase Imaging with Digital Holographic Microscopy Accurately Assesses Intestinal Inflammation and Epithelial Wound Healing. *Journal of Visualized Experiments.* (115), (2016).
25. Huang, J., Guo, P., Moses, M. A. A Time-lapse, Label-free, Quantitative Phase Imaging Study of Dormant and Active Human Cancer Cells. *Journal of Visualized Experiments.* (132), (2018).
26. Yang, S. A., Yoon, J., Kim, K., Park, Y. Measurements of morphological and biochemical alterations in individual neuron cells associated with early neurotoxic effects in Parkinson's disease. *Cytometry Part A.* **91**(5), 510-518 (2017).
27. Cotte, Y., *et al.* Marker-free phase nanoscopy. *Nature Photonics.* **7**(2), 113-117 (2013).
28. Nguyen, T. H., Kandel, M. E., Rubessa, M., Wheeler, M. B., & Popescu, G. Gradient light interference microscopy for 3D imaging of unlabeled specimens. *Nature Communications.* **8**(1), 210 (2017).
29. Kwon, S. *et al.* Mitochondria-targeting indolizino [3, 2-c] quinolines as novel class of photosensitizers for photodynamic anticancer activity. *European Journal of Medicinal Chemistry.* **148 ,**116-127 (2018).
30. Bennet, M., Gur, D., Yoon, J., Park, Y., Faivre, D. A Bacteria-Based Remotely Tunable Photonic Device. *Advanced Optical Materials.* (2016).
31. Kim, T. I., *et al.* Antibacterial Activities of Graphene Oxide-Molybdenum Disulfide Nanocomposite Films. *ACS Applied Materials & Interfaces.* **9**(9), 7908-7917 (2017).
32. Bedrossian, M., Barr, C., Lindensmith, C. A., Nealson, K., Nadeau, J. L. Quantifying Microorganisms at Low Concentrations Using Digital Holographic Microscopy (DHM). *Journal of Visualized Experiments.* (129), (2017).
33. Jo, Y., *et al.* Quantitative Phase Imaging and Artificial Intelligence: A Review. *arXiv preprint arXiv:1806.03982.* (2018).
34. Javidi, B., Moon, I., Yeom, S., Carapezza, E. Three-dimensional imaging and recognition of microorganism using single-exposure on-line (SEOL) digital holography. *Optics Express.* **13**(12), 4492-4506 (2005).
35. Jo, Y., *et al.* Label-free identification of individual bacteria using Fourier transform light scattering. *Optics Express.* **23**(12), 15792-15805 (2015).
36. Jo, Y., *et al.* Angle-resolved light scattering of individual rod-shaped bacteria based on Fourier transform light scattering. *Scientific Reports.* **4 ,**5090 (2014).
37. Jo, Y., *et al.* Holographic deep learning for rapid optical screening of anthrax spores. *Science Advances.* **3**(8), e1700606 (2017).
38. Mirsky, S. K., Barnea, I., Levi, M., Greenspan, H., Shaked, N. T. Automated analysis of individual sperm cells using stain-free interferometric phase microscopy and machine learning. *Cytometry Part A.* **91**(9), 893-900 (2017).
39. Roitshtain, D., *et al.* Quantitative phase microscopy spatial signatures of cancer cells. *Cytometry Part A.* **91**(5), 482-493 (2017).
40. Lam, V. K., Nguyen, T. C., Chung, B. M., Nehmetallah, G., Raub, C. B. Quantitative assessment of cancer cell morphology and motility using telecentric digital holographic microscopy and machine learning. *Cytometry Part A.* (2017).
41. Pavillon, N., Hobro, A. J., Akira, S., Smith, N. I. Noninvasive detection of macrophage activation with single-cell resolution through machine learning. *Proceedings of the National Academy of Sciences.*201711872 (2018).
42. Basu, S., Campbell, H. M., Dittel, B. N., Ray, A. Purification of Specific Cell Population by Fluorescence Activated Cell Sorting (FACS). *Journal of Visualized Experiments.* (41), e1546 (2010).
43. Takeda, M., Ina, H., Kobayashi, S. Fourier-transform method of fringe-pattern analysis for computer-based topography and interferometry. *Journal of the Optical Society of America*. **72**(1), 156-160 (1982).
44. Debnath, S. K., Park, Y. Real-time quantitative phase imaging with a spatial phase-shifting algorithm. *Optics Letters.* **36**(23), 4677-4679 (2011).
45. Kim, K., *et al.* High-resolution three-dimensional imaging of red blood cells parasitized by Plasmodium falciparum and in situ hemozoin crystals using optical diffraction tomography. *Journal of Biomedical Optics.* **19**(1), 011005 (2013).
46. Vercruysse, D., *et al.* Three-part differential of unlabeled leukocytes with a compact lens-free imaging flow cytometer. *Lab on a Chip.* **15**(4), 1123-1132 (2015).
47. Kim, K., *et al.* Correlative three-dimensional fluorescence and refractive index tomography: bridging the gap between molecular specificity and quantitative bioimaging. *Biomedical Optics Express.* **8**(12), 5688-5697 (2017).
48. Shin, S., Kim, D., Kim, K., Park, Y. Super-resolution three-dimensional fluorescence and optical diffraction tomography of live cells using structured illumination generated by a digital micromirror device. *arXiv preprint arXiv:1801.00854.* (2018).

49. Chowdhury, S., Eldridge, W. J., Wax, A., Izatt, J. A. Structured illumination multimodal 3D-resolved quantitative phase and fluorescence sub-diffraction microscopy. *Biomedical Optics Express.* **8**(5), 2496-2518 (2017).